ICES Journal of Marine Science

ICES Journal of Marine Science (2021), https://doi.org/10.1093/icesjms/fsab183

Original Article

Mesopelagic flesh shear viscosity estimation from *in situ* broadband backscattering measurements by a viscous–elastic model inversion

Babak Khodabandeloo [1,*], Mette Dalgaard Agersted [2], Thor A. Klevjer[2], Geir Pedersen [1], and Webjørn Melle[2]

[1]*Ecosystem Acoustics Research Group, Institute of Marine Research, P.O.Box 1870, Nordnes, NO-5817 Bergen , Norway*
[2]*Plankton Research Group, Institute of Marine Research, P.O.Box 1870, Nordnes, NO-5817 Bergen, Norway*

[*]*Corresponding author: tel: +4745078868; e-mail: khodabandeloo.babak@gmail.com*

Khodabandeloo, B., Agersted, M. D., Klevjer, T. A., Pedersen, G., and Melle, W. Mesopelagic flesh shear viscosity estimation from *in situ* broadband backscattering measurements by a viscous–elastic model inversion. – ICES Journal of Marine Science, 0: 1–15.

Received 12 April 2021; revised 11 August 2021; accepted 27 August 2021.

In fisheries acoustics, target strength (*TS*) is a key parameter in converting acoustic measurements to biological information such as biomass. Modelling is a versatile tool to estimate *TS* of marine organisms. For swimbladdered fish, flesh shear viscosity is one of the required parameters to correctly calculate *TS* around the resonance frequency, where the target scatters most strongly. Resonance of mesopelagic swimbladdered fish can occur over a range of frequencies and can be within commonly used frequencies (e.g. 18, 38, or 70 kHz). Since there is little information on flesh shear viscosity of fish, especially for mesopelagic species, their resonance can bias the biological information extracted from acoustic measurements. Here, first, the applicability of using a spherical model to estimate resonant backscattering of a generic swimbladder is investigated. Subsequently, a viscous–elastic spherical gas backscattering model is used to estimate the flesh shear viscosity of swimbladdered mesopelagic fish (most likely *Cyclothone* spp., Family: Gonostomatidae) from *in situ* broadband backscattering measurements. Finally, the effects of flesh shear viscosity on the *TS* of swimbladdered mesopelagic fish at 18, 38 (a widely used channel to study mesopelagic layers), and 70 kHz are examined.

Keywords: broadband, mesopelagic fish, modeling, resonance, shear viscosity, swimbladder, target strength.

Introduction

Mesopelagic fish are believed to play a key role in carbon flux and biochemical processes in the oceans (Davison *et al.*, 2013; Irigoien *et al.*, 2014). In addition, their suitability as a food source for humans and a major source of fatty acids and protein is under investigation (Robinson *et al.*, 2010; Alvheim *et al.*, 2020). However, there is at least one order of magnitude uncertainty in our current estimates of their biomass, which restricts understanding of their actual significance and suitability for commercial exploitation (Gjoesaeter and Kawaguchi, 1980; Irigoien *et al.*, 2014; Davison *et al.*, 2015b). Active acoustic methods are essential tools in pelagic fishery surveys and may be more efficient than other methods such as trawls and optical cameras in estimating densities of organisms at mesopelagic depths (Kaartvedt *et al.*, 2012). Acoustic sampling provides vast amounts of data that can potentially be used for both qualitative and quantitative observations of marine organisms over large spatial and temporal scales (Simmonds and MacLennan, 2005; Kloser *et al.*, 2009). Fisheries acoustic technologies have matured over time, and the availability of advanced and sophisticated digital hardware has catalysed the research in this area (Chu, 2011). Yet, one of the main challenges regarding acoustic methods is to interpret the collected acoustic data to identify and size the targets.

Target strength (*TS*) is a logarithmic measure of the backscattering cross-section, which is the backscattering from a single acous-

tic target. It is a key parameter in quantitative analyses of acoustic data in fisheries acoustics (Ona, 1999). For acoustic data collection, a transducer transmits controlled acoustic pulses and records the reflected acoustic waves (the backscattered pressure) by the insonified targets. The backscattering depends in a complex manner on the target size (compared to the wavelength of incident acoustic wave), shape, orientation, and its material properties (Faran, 1951; Hickling, 1962; Stanton *et al.*, 1998). These features can be very different among aquatic organisms. To adequately characterize the marine organisms acoustically, a reasonable approach has been to categorize the organisms per gross anatomical features into gas-bearing, elastic-shelled, and quasi-fluid (Medwin, 2005; Lavery *et al.*, 2007; Stanton *et al.*, 2010). Resonant scattering by gas-bearing organisms is one of the main issues that complicates the analysis of the acoustic data for biomass estimation (Davison *et al.*, 2015a). A gas-filled organ is a strong sound reflector and accounts for more than 90% of the total backscattering (Foote, 1980) of an organism, if such an organ is present. Resonant scattering by swimbladder-bearing fish frequently dominates the backscattering in the lower frequencies (Love, 1978). For epipelagic fish, the resonant frequency is expected to be around 1–25 kHz. On the other hand, for mesopelagic species, the resonance frequency can occur at higher frequencies due to smaller swimbladder size and higher density of its gas content due to the depth (Khodabandeloo *et al.*, 2021a). To convert measured backscattering into biologically meaningful quantities such as biomass, backscattering models are useful (Love, 1978; Ona, 1999; Horne, 2000; Reeder *et al.*, 2004).

Shear viscosity is one of the material properties that characterizes the resistance to shear deformation (Baidakov *et al.*, 2011). Shear viscosity of the fish flesh affects the backscattered amplitude around the resonance frequencies of swimbladder-bearing fish (Scoulding *et al.*, 2015; Davison *et al.*, 2015a). However, there is little information for fish tissue (Love, 1978; Feuillade and Nero, 1998; Scoulding *et al.*, 2015; Proud *et al.*, 2019), especially for mesopelagic species. Using incorrect values for the flesh shear viscosity causes under- or over-estimation of the *TS*. This subsequently biases the estimates obtained from analysing the collected acoustic data by using backscattering models.

A viscous–elastic model, based on the model presented by Feuillade and Nero (1998), has been demonstrated to be able to describe frequency responses from mesopelagic fish measured over wideband frequencies (38 and ∼50–250 kHz) in the field (Khodabandeloo *et al.*, 2021a). The model has 12 tunable parameters, and fitting the model to measured frequency responses from swimbladdered fish *in situ* resulted in estimates of swimbladder sizes of the fish. However, the model can also be used for the estimation of other parameters, such as flesh shear viscosity.

In the present study, the aim is to estimate the flesh shear viscosity of swimbladdered mesopelagic fish from broadband acoustic field data. Since swimbladders usually have a non-spherical shape, at first, the applicability of spherical model to study resonance of non-spherical gas-filled shapes is investigated. In this regard, a finite element model (FEM), providing a numerical solution to model backscattering pressures of arbitrary shapes is used (Jech *et al.*, 2015). Subsequently, flesh shear viscosity of mesopelagic fish was estimated by fitting the viscous–elastic gas-filled sphere model to *in situ* measured wideband (38 and ∼50–250 kHz) *TS* spectra of mesopelagic fish. Furthermore, the effects of flesh shear viscosity on the *TS* of swimbladdered mesopelagic fish are studied at frequencies that are used by most fishery surveys to monitor the mesopelagic layers.

Material, methods, and results

Field *TS* measurements

TS of mesopelagic organisms used in this paper was collected in the eastern part of Mid-Atlantic Ocean, offshore Morocco, during a research cruise on board R/V Kronprins Haakon (Norwegian Institute of Marine Research, IMR) in (2—22) May 2019. An underwater vehicle, MESSOR (Knutsen *et al.*, 2013), was towed behind the ship, performing oblique hauls from 0 to 1000 m depth at a horizontal speed of ∼2 m s^{-1}. It was equipped with a four-channel echosounder system (Simrad EK80 WBT Tubes) with multiple downward-looking split-beam transducers: one 38 kHz narrowband and three broadband with centre frequencies of 70, 120, and 200 kHz. In addition, the MESSOR was equipped with a conductivity, temperature, and depth (CTD) profiler (Seabird SBE 49 FastCAT). The echosounder settings can be found in Khodabandeloo *et al.* (2021a) and are repeated in Supplementary Table S1 in the supplementary material. The observation range was limited to 60 m and the echosounders were pinging simultaneously with 3–4 pings per second. Acoustic interference between the channels (crosstalk) was reduced by adjusting the power settings (Khodabandeloo *et al.*, 2021b).

Based on acoustic measurements from MESSOR, single targets were manually selected from a depth of ∼500 to 900 m at a station located from 30.31°N 13.49°W to 30.37°N 13.34°W. Only those targets that had the primary resonance within the measured broadband frequencies were selected for parameter estimation with the focus on flesh shear viscosity. Further analyses and background information on the acoustic data can be found in Khodabandeloo *et al.*, (2021a). Biological sampling using a macroplankton trawl (García-Seoane *et al.*, 2021) and Multinet suggests that the dominating micronekton genus within the depth strata at this station was *Cyclothone* spp. (Family: Gonostomatidae), which is one of the world's most numerous vertebrates (Nelson *et al.*, 2016).

Finite element backscattering model of arbitrary shape axisymmetric swimbladders

It is more likely for a swimbladder to have ellipsoidal or irregular shape than being a sphere (e.g. Marshall, 1960). To calculate the backscattering of a non-spherical swimbladder, numerical methods are required since analytical solutions either do not exist or are complicated. One of the powerful numerical methods for backscattering estimation of an object with an arbitrary shape is finite element method (FEM). It has the potential to provide highly accurate estimates but is computationally expensive (Jech *et al.*, 2015). To investigate the effects of swimbladder shape on the backscattering, a frequency-domain FEM was implemented by using COMSOL Multiphysics® V.5.4. To reduce the computational cost, axisymmetric swimbladders were studied that enable us to solve a 2D axisymmetric problem (adapted from Zampolli *et al.*, 2007; Bonomo and Isakson, 2016) instead of a full 3D problem. The memory requirements for a 2D model are much less than a 3D model (Ida, 1983), which is specifically important for backscattering estimation at high frequencies (Antona, 2016). Backscattering from five different axially symmetric swimbladders (Figure 1) with the same volume subjected to a planar acoustic wave was estimated over the frequency range of 0.5–400 kHz with a frequency spacing of 0.25 kHz.

To include the planar incident wave in an axisymmetric model, the Jacobi–Anger expansion is used (Cakoni and Colton, 2005),

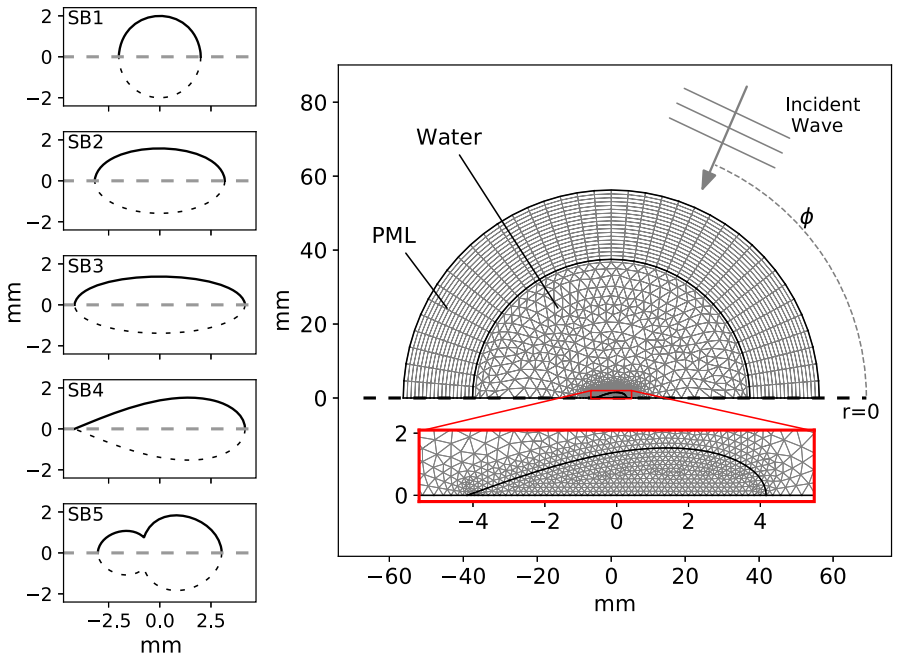

Figure 1. (Left) Different swimbladder shapes (SB1–5) but with the same volume as a sphere of 2 mm radius. SB1 is a sphere and SB2 and SB3 are prolate spheroids with the aspect ratio of 2 and 3, respectively. (Right) 2D axisymmetric FEM, using SB4 as an example of swimbladder shape. The computational domain is surrounded by a perfectly matched layer (PML) to diminish the reflections of the waves from the domain boundary. The symmetry axis (r = 0) is shown by the dashed line and is the incident angle.

which expands a planar wave (e.g. propagating in x-direction) in a series of cylindrical waves (r and θ):

$$e^{ikx} = e^{ikr\cos\theta} = \sum_{m=-\infty}^{+\infty} i^m J_m(kr)\, e^{im\theta}, \tag{1}$$

where k is the wave number and J_m refers to the m*th* Bessel functions of the first kind. First 11 terms ($m = 0, 1, 2, \ldots, 10$) were used to estimate the backscattering. To benchmark the finite element solution, backscattering of the sphere (SB1) by FEM was compared to that of analytical modal solution (Anderson, 1950; Figure 2) with 21 backscattering modes. The agreement between them validates the implementation of FE modelling and the adequacy of 11 terms in this example.

Then the *TS* is constructed by adding the backscattering of each individual terms as

$$TS = 20\log_{10}\left(\sum_{m=0}^{N-1} r p_m(r)/p_{inc}\right), \tag{2}$$

where $p_m(r)$ is the backscattered pressure at range r for the term m, p_{inc} is the incident pressure amplitude, and N is the number of terms included in the backscattering calculation.

Effects of swimbladder shape on the backscattering

Broadside backscattering (i.e. $\phi = 90^\circ$ in Figure 1) for five swimbladders SB1–5 (Figure 1) were estimated between 0.5 and 400 kHz at discrete frequencies spaced 0.25 kHz (Figure 2) using FEM. The density and sound speed of the swimbladder were assumed to be 80 kg m^{-3} and 325 m s^{-1}, respectively. Surrounding water density and sound speed were 1027 kg m^{-3} and 1500 m s^{-1}, respectively. The overlap between the estimated backscattering of the sphere (SB1) from FEM and modal solution validates the FEM implementation. Furthermore, the shift in the resonance frequency of prolate spheroids (SB2 and SB3 in Figure 2) with respect to that of their spherical counterparts (i.e. the same volume sphere) estimated by FEM (SB1 in Figure 2) is compared (Table 1) to the values obtained by the Ye (1997) formula see Equation (S1). To improve the accuracy of finding the resonance frequency, a spline was fitted to the discrete *TS* values (frequency resolution = 0.25 kHz) obtained by FEM around the peak.

For different shapes (SB1−5), the resonance frequencies vary between 12442 and 13054 Hz and the peak *TS* values are within −34.4 and −34.8 dB. It is seen that around the main resonance frequencies, unlike the higher frequency region, the *TS* frequency response is not considerably affected by the swimbladder shape (Figure 2). For frequencies beyond approximately four times the resonance frequency, the spherical swimbladder (SB1) resulted in lower *TS* values compared to the broadside backscattering from elongated swimbladders (SB2–5).

Effects of swimbladder orientation on the backscattering

The target orientation is usually unknown when measuring its acoustic backscattering in the field. Therefore, it is necessary to know at which frequencies and how much the target orientation affects the backscattered wave. This is studied by estimating the backscattering of the prolate spheroid with the aspect ratio of 3 (SB3) for different incident angles, ϕ (Figure 3).

It is observed that around the resonance frequencies, the *TS* frequency response is independent of the incident angle. One the other hand, it has significant effects on the *TS* frequency response in the higher frequency region (e.g. up to ∼15 dB). Highest estimated *TS*

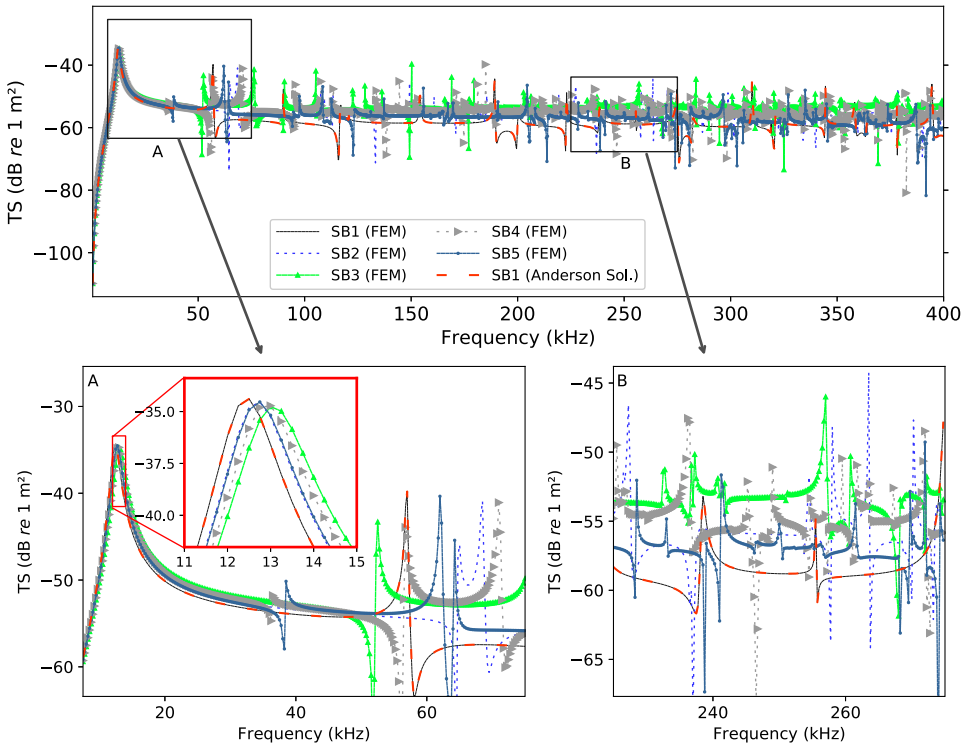

Figure 2. (Top) Estimated broadside ($\phi = 90^o$) backscattering for five different swimbladder shapes (SB1–5, Figure 1) using a 2D axisymmetric FEM implemented in COMSOL Multiphysics using 11 terms in Equation (1). For the spherical swimbladder (SB1), backscattering is also calculated using the Anderson model (Anderson, 1950) with 21 modes. Resonance and a higher frequency region are zoomed by "A" and "B", respectively. The targets were assumed to be at a depth of around 550 m. Density and sound speed of gas are assumed to be 80 kg m^{-3} and 325 m s^{-1}, respectively, and 1027 kg m^{-3} and 1500 m s^{-1}, respectively, for water.

Table 1. Resonance frequency ratio "$\omega_{0\epsilon}/\omega_0$" for a prolate spheroidal bubble compared to the sphere of the same volume from the FEM and Ye (1997) formula. $\omega_{0\epsilon}$ and ω_0 are the resonance frequencies of the prolate spheroid and sphere of the same volume, respectively.

		FEM (Figure 2)	(Ye, 1997)	Difference (%)
$\omega_{0\epsilon}/\omega_0$	Aspect ratio = 2	1.020	1.022	0.196
	Aspect ratio = 3	1.049	1.055	0.572

values were obtained when the incident angle was 90°, and *TS* decreased with decreasing incident angle.

In summary, the studied backscattering from the swimbladder examples in this section indicates that resonance frequencies vary up to 5% from the spherical one. In addition, orientation has no effect on the backscattering around the resonance frequencies. Therefore, spherical models can be useful to study the *in situ* measured swimbladder backscattering around the resonance frequency even if their shapes and orientations are unknown.

Viscous–elastic swimbladder model

One of the backscattering models that includes fish flesh shear viscosity is a two-layer viscous–elastic mathematical/physical spherical model (Feuillade and Nero, 1998). It was used to model the backscattering from swimbladder-bearing mesopelagic organisms (Khodabandeloo *et al.*, 2021a). In this model (Figure 4), a spherical gas bubble with an elastic shell, which represents the swimbladder and swimbladder wall, respectively, is surrounded by a viscous layer representing the fish flesh.

Explanation of model parameters is briefly repeated here, but for a detailed description of the model's governing equations and parameters, see Khodabandeloo *et al.* (2021a). It requires 12 parameters to estimate backscattering (see Supplementary Table S2 in supplementary material). Some of the model parameters are either based on a thermodynamic law and experimental equations or have minimal effect on the backscattering. For example, sound speed (c_{SB}) and density (ρ_{SB}) of the gas inside the swimbladder, which is assumed to be filled by oxygen (Ross, 1976; Priede, 2017), are calculated using the pertinent equations for the given pressure and temperature provided by *in situ* conductivity, temperature, and depth (CTD) measurements (Khodabandeloo *et al.*, 2021a). Sound speed (c_w) and density (ρ_w) of the surrounding seawater are a function of pressure, temperature, and salinity (see Appendix A in Massel, 2015). Parameters such as flesh density (ρ_f), sound speed (c_f), and swimbladder wall tissue density (ρ_{SBW}) are known to be confined to the limited range of values based on experimental measurements and have secondary effects on the overall backscattering. Another parameter is flesh thickness, which has a minor effect on the backscattering around the resonance (see the section

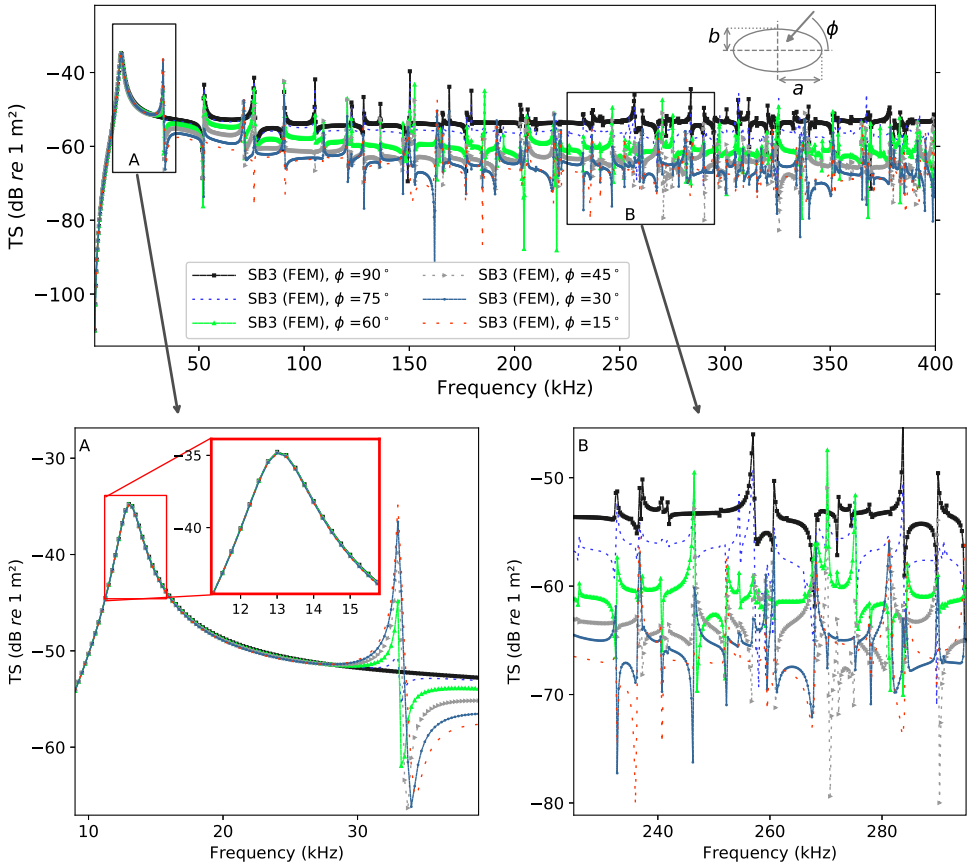

Figure 3. Estimated backscattering for a prolate spheroid swimbladder (SB3) for six different incident angles $\phi = 90$ (broadside incident), 75, 60, 45, 30, and 15° by FEM. Zoomed regions around the resonance and higher frequencies are labelled by "A" and "B", respectively.

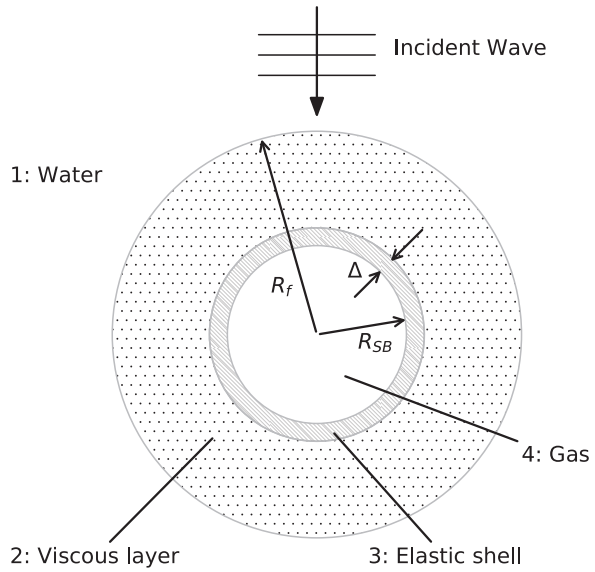

Figure 4. Viscous–elastic two-layer spherical swimbladder model (Khodabandeloo *et al.*, 2021a). R_{SB} is the swimbladder equivalent spherical radius (ESR), Δ is the swimbladder wall thickness, and R_f is the ESR of fish flesh.

"Model parameters effects on *TS* around resonance"). Swimbladder wall thickness and its shear elasticity vary between species, juveniles, and adults (Marshall, 1960). Flesh shear viscosity influences the resonance amplitude, but there is limited information for mesopelagic species. Swimbladder size has a significant effect on the overall backscattering (Khodabandeloo *et al.*, 2021a).

Model parameters effects on TS around resonance

Effects of four model parameters, i.e. swimbladder radius, R_{SB}, swimbladder wall thickness, Δ, its shear elastic modulus, μ_{SBW}, and flesh shear viscosity, μ_f, on the backscattering are shown for a shallow (50 m) and deep (500 m) occurring target, focusing on the resonant region of the two targets (Figure 5). Each of the parameters are changed at a time, using values reported in the literature (see e.g. Tables 3–5 in Khodabandeloo *et al.*, 2021a), and their effect(s) on the backscattering are observed by comparing C2–5 to the backscattering from the base model shown by solid black line (C1). The backscattering is most sensitive to the swimbladder size (R_{SB}) and flesh shear viscosity (μ_f) variations. The former one affects resonance location and the latter one influences resonance amplitude. For example, changing the flesh shear viscosity, μ_f, from 1.0 to 3.0 kg m^{-1} s^{-1} (curves C1 and C5) resulted in a more damped/flattened resonance region. The decrease in *TS* level at the resonance peak was more pronounced for the shallow-occurring target. A smaller swimbladder radius (C2) resulted in a higher resonance frequency

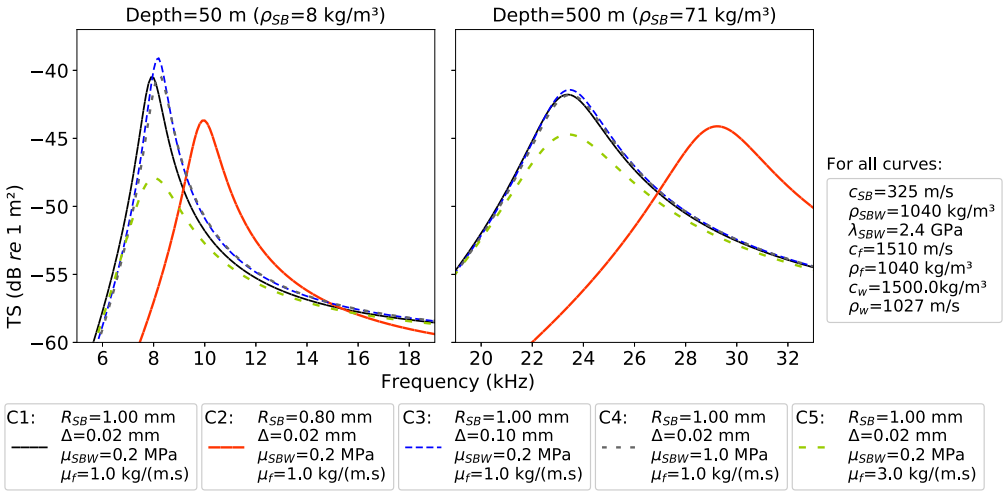

Figure 5. Calculated backscattering from the viscous–elastic spherical swimbladder model for a shallow (50 m; left panel) and deep (500 m; right panel) target. Effects of R_{SB} (C2), Δ (C3), μ_{SBW} (C4), and μ_f (C5) on the backscattering are observed by comparing the curves to the base model (C1). The common parameters for all cases are given on the right side of the figure.

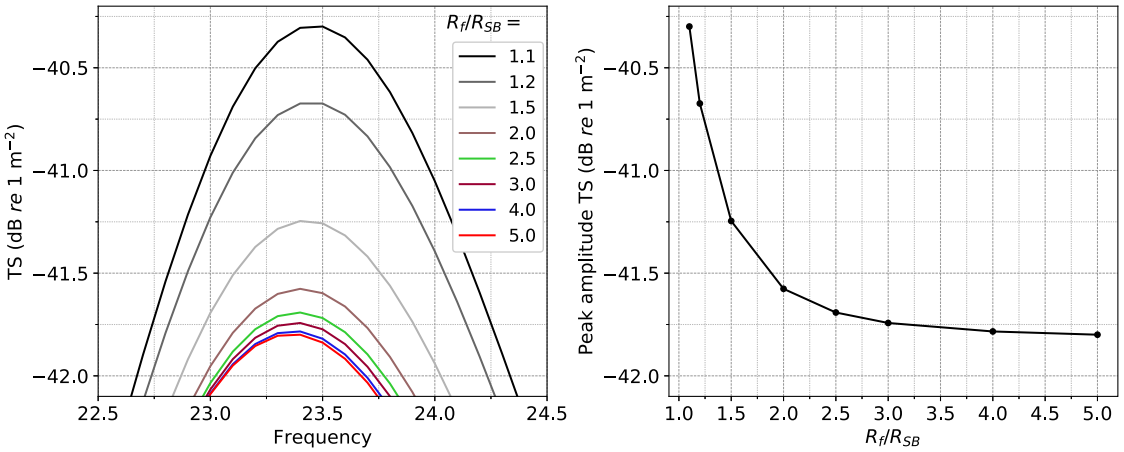

Figure 6. (Left) Backscattering around the resonance frequency for eight different flesh thicknesses, presented as a ratio between fish flesh and swimbladder radius (R_f/R_{SB}). (Right) The peak amplitude of backscattering for eight different flesh thicknesses. The model parameters are $R_{SB} = 1$ mm, $\Delta = 0.02$ mm, $\rho_{SB} = 71\,\mathrm{kg\,m^{-3}}$, $c_{SB} = 325\,\mathrm{m\,s^{-1}}$, $\mu_{SBW} = 0.2$ MPa, $\mu_f = 1\,\mathrm{kg\,m^{-1}\,s^{-1}}$, $\rho_w = 1027\,\mathrm{kg\,m^{-3}}$, $c_w = 1500\,\mathrm{m\,s^{-1}}$, $\rho_{SBW} = 1040\,\mathrm{kg\,m^{-3}}$, $\rho_f = 1040\,\mathrm{kg\,m^{-3}}$, $c_f = 1510\,\mathrm{m\,s^{-1}}$, and $c_{SBW} = 1520\,\mathrm{m\,s^{-1}}$. The flesh thickness is $R_f - R_{SB} - \Delta$ and is given for eight different values (i.e. $R_f/R_{SB} = 1.1$, 1.2, 1.5, 2.0, 2.5, 3.0, 4.0, and 5.0).

and lower *TS* both at the resonance peak and at higher frequencies (data not shown for the latter). The thickness of the swimbladder wall (C3) and its shear elasticity (C4) had minor effects on the resonance amplitude and resonance frequency, especially for the deeper target. Swimbladder wall thickness and its shear elasticity depend on the species and are reported for few species (see Tables 4 and 5 in Khodabandeloo *et al.*, 2021a).

In addition to the four parameters studied in this section, flesh thickness effects on the resonance backscattering are studied (Figure 6). The sensitivity of resonant backscattering to the flesh thickness is studied through an example (Figure 6). The backscattering from the viscous–elastic model is simulated for eight different flesh thicknesses, while the rest of model parameters were unchanged. It is observed that for a thin layer of flesh thickness ($R_f/R_{SB} < 1.5$), the backscattering is more sensitive to the flesh thickness. On the other hand, beyond a certain flesh thickness ($R_f/R_{SB} >\sim 2$), its increase has minor effect on the backscattering amplitude. The dependence of backscattering on the shell thickness has been studied by Baik (2013) for different gas bubble radii and similar results were reported. It is worth noting that *TS* amplitude variations are less than ∼1.5 dB between the smallest and largest flesh thicknesses.

Automated curve-fitting

Parameters of the viscous–elastic model can be tuned such that the *TS* frequency response from modelling resembles the measured one (Khodabandeloo *et al.*, 2021a). This process can be automated using an optimization algorithm. Here, "least_squares" function, which is a nonlinear least-squares algorithm from the optimization module of "SciPy v1.7.0" (Jones *et al.*, 2001), a Python library, was used. The algorithm finds the local minimum of the cost function by solving

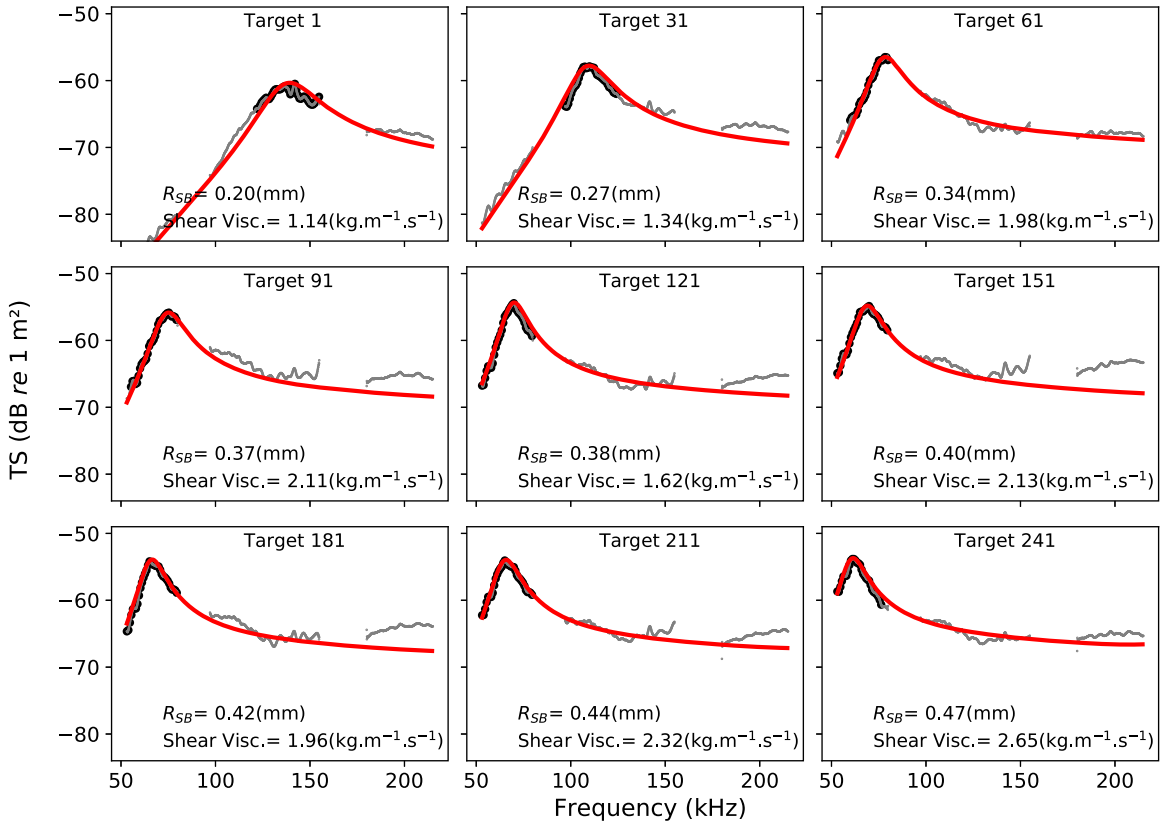

Figure 7. Data and model for shear elastic modulus of 0.2 MPa and swimbladder wall thickness of 20 μm. The swimbladder radius and flesh shear viscosity, which provide the best match around the resonance between the modelled and measured *TS* frequency responses, are given. Estimated swimbladder radii of the targets are listed from smallest (upper left graph) to largest (lower right graph).

a nonlinear least-squares problem within the given bounds for the independent variables.

Many of the parameters were selected per thermodynamic laws or based on previously reported biological values from the literature (for details, see Khodabandeloo *et al.*, 2021a). The optimization variables were swimbladder radius (R_{SB}) and the flesh shear viscosity (μ_f). To increase the chance of finding global minimum within the given bounds, the optimization was performed for three different initial values of the optimization variables as (0.15, 0.5), (0.25, 0.5), and (0.25, 2), where the first parameter represents swimbladder radius (mm) and the second parameter is shear viscosity (kg m^{-1} s^{-1}).

Model-fitting to in situ *TS measurements for flesh shear viscosity estimation*

Single targets with main resonance within the measured broadband frequencies were selected for parameter estimation with the focus on flesh shear viscosity. The fitting of the model to the measured *TS* values are shown for nine (among 247) selected targets after sorting the estimated swimbladder radii in ascending order. The fitting was performed only for the frequency band around the resonance (indicated by bold black dots in Figure 7). The swimbladder radius and flesh shear viscosity are obtained through optimization (curve-fitting) and shown for each target in their panel. In Figure 7, the swimbladder wall thickness and its shear elastic modulus were assumed 20 microns and 0.2 MPa, respectively.

Of the values applied in Figure 5, thickness and shear elastic modulus of the swimbladder wall have limited effects on *TS* around the resonance region. Since these two parameters are unknown for many mesopelagic species, the optimization problem is solved for three different swimbladder wall shear elastic moduli, 0.2, 1, and 2 MPa and three swimbladder wall thicknessess of 20, 100, 200 microns, which provide nine different combinations. The fitting quality is quantified by the fitting error, which is the mean square of differences between the modelled and measured *TSs* at the frequencies used for the curve fitting, divided by the number of frequencies used for fitting. For some targets, the resonance frequency was near the edge of the measured broadband frequencies and therefore fewer points were used for the curve fitting. The fitting error for each target is normalized to the largest value of the nine different cases and is called column-wise fitting error (Figure 8). The fitting error normalized to the largest fitting error of all targets is called global normalized fitting error (Figure 8). From the column-wise normalized fitting error, it is observed that swimbladder wall thickness of 20 microns gives the best fitting quality irrespective of the shear elasticity of the swimbladder wall (smaller normalized fitting error). In addition, the lower values of shear elasticity (softer) provide better fitting quality than the higher ones (stiffer). The global normalized fitting error shows that except for a few targets, the majority of targets have almost similar quality of fitting (Figure 8).

For the case where swimbladder wall thickness and shear elasticity were assumed 20 μm and 0.2 MPa, respectively, the estimated

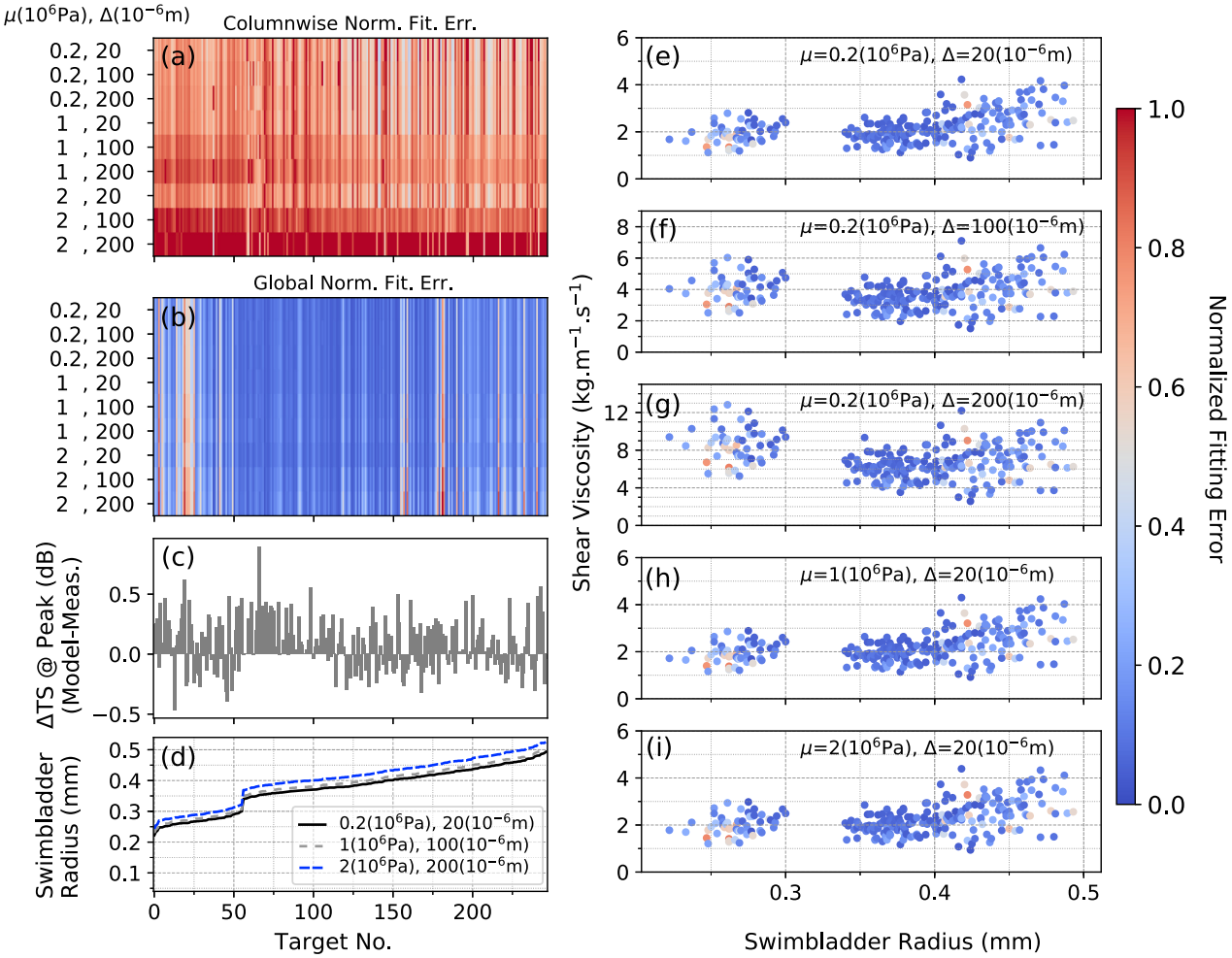

Figure 8. Estimated flesh shear viscosities and swimbladder radii from fitting the model to the measured *TS* of selected ($N = 247$) targets for different combinations of swimbladder wall thicknesses and shear elastic moduli. The fitting errors are normalized column-wise (a) and global (b). For the column-wise normalization, the values of each column are normalized to the largest value of the column. For the global normalization, the values are normalized to the largest value of the entire matrix. (c) Difference between modelled and measured peak *TS*s. Estimated swimbladder radius (d) for three different cases indicated in the graph after sorting targets in ascending order (i.e. starting with the target having the smallest swimbladder radius). (e–i) Estimated flesh shear viscosity for five different combimations of swimbladder wall shear elasticity and flesh shear viscosity (denoted on each panel) with the global error colour bar. Note the different *y*-axes for subplots "e–i".

flesh shear viscosity values and swimbladder sizes are chosen for further analysis (Figure 9). Note that targets with swimbladder radius between ∼0.3 and 0.34 mm are not present in the data. The reason is that those targets have resonance within the unmeasured or excluded frequency band ∼80-97 kHz and were therefore not selected for viscosity estimation.

A regression line is fitted to the data, and slope, intercept, and the corresponding standard errors are obtained using "linregress" (version 1.7.0) function from the statistical package of "SciPy" (Jones *et al.*, 2001), a Python library. The relation is given by

$$\mu_f = (3.86 \pm 0.53)\, R_{SB} + (0.68 \pm 0.20)\,, \tag{3}$$

where R_{SB} is in mm and μ_f in kg m^{-1} s^{-1}. The linear model together with confidence and prediction intervals (Weisberg, 2014, chapter 2) are shown in Figure 9.

The linear regression model can also be expressed by the standard error of regression, ε, and R^2 value as

$$\mu_f = 3.86 R_{SB} + 0.68 \pm \varepsilon, \quad \varepsilon = 0.57,\ R^2 = 0.17, \tag{4}$$

where the standard error of regression is calculated by (Weisberg, 2014, chapter 2)

$$\varepsilon = \sqrt{\frac{\sum \left(\mu_{f\,meas.} - \mu_{f\,model.}\right)^2}{N-2}}. \tag{5}$$

In this formula, the measured and modelled flesh shear viscosity are shown by the corresponding subscripts, and N is the number of measured values (here 247).

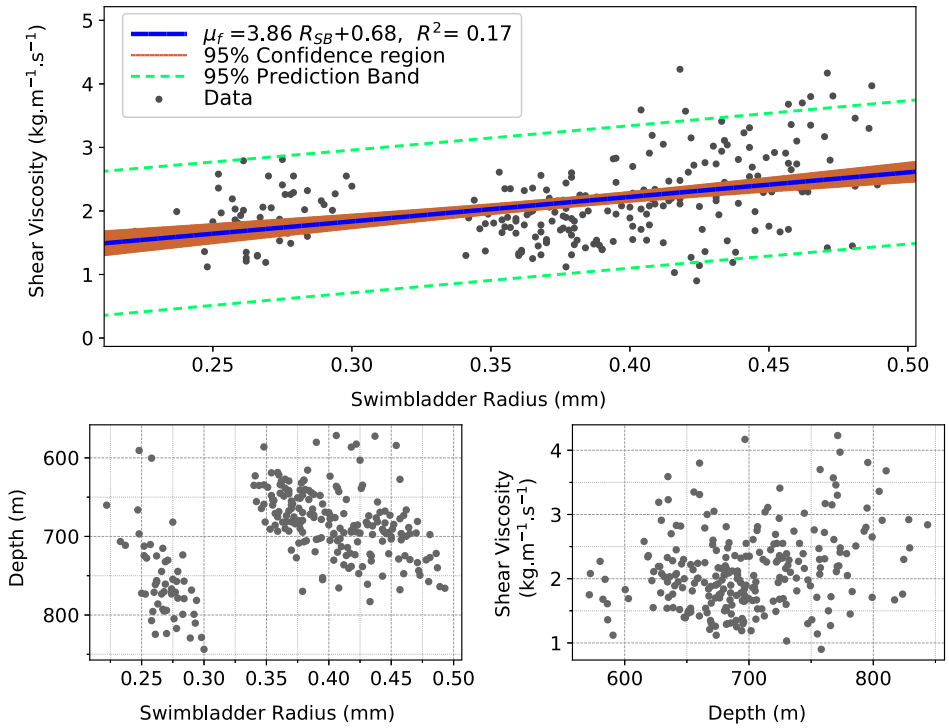

Figure 9. Estimated flesh shear viscosity for 247 single targets as a function of their estimated swimbladder radius (top). Regression line (Equation (3)), and confidence and prediction intervals. Depth vs. estimated swimbladder radius (lower left). Estimated flesh shear viscosity vs. target depth (lower right). In the model, the swimbladder wall thickness and shear elasticity are assumed to be 20 μm and 0.2 MPa, respectively.

Evaluation of the estimated flesh shear viscosity for larger targets

The flesh shear viscosity model (i.e. Equation (3)) was evaluated for larger targets (Figure 10) to check its performance when extrapolated beyond the swimbladder sizes (radii) used to estimate the flesh shear viscosity displayed in Figure 9. Larger single targets with resonance at lower frequencies than 53-kHz, the lower frequency limit of the 70-kHz channel used in this paper, were selected. The measured *TS* by the narrowband 38-kHz channel is included together with the 70, 120, and 200 kHz broadband measurements. Subsequently, viscous–elastic model was fitted to the measured *TS* at 70-kHz band (53–80 kHz) where the optimization parameter was swimbladder radius. The flesh shear viscosity is a function of the swimbladder radius per Equation (3). Thickness and shear elasticity of swimbladder wall were assumed constant values, 20 μm and 0.2 MPa, respectively.

TS variation at 18, 38, and 70 kHz for different flesh shear viscosity values

Mesopelagic layers can be reached by lower frequency acoustic channels (i.e. 18, 38, and 70 kHz) measuring from the surface. Among them, 38 kHz frequency has been widely used (e.g. Klevjer *et al.*, 2012; Irigoien *et al.*, 2014; Proud *et al.*, 2019). Here, we will study the effects of flesh shear viscosity on the *TS* of swimbladdered fish at these frequencies (18, 38, and 70 kHz). Flesh shear viscosity affects resonance amplitude, and the resonance frequency of a swimbladder depends on its depth (see e.g. Figure 5). Hence, *TS* for a range of swimbladder sizes (quantified by equivalent spherical radius, ESR) at three different mesopelagic depths 200, 500, and 800 m is estimated using the obtained model (Equation (3)) and four constant shear flesh viscosity values for three acoustic frequencies 18, 38, and 70 kHz. (Figures 11–13). It is observed that at a given frequency, maximum backscattering happens for larger targets by increasing the depth. Furthermore, the resonance backscattering amplitude is more sensitive to the flesh shear viscosity values for targets at shallower depth.

Discussion

Flesh shear viscosity of mesopelagic fish is estimated from *in situ* measured broadband backscattering by an inverse method. The flesh shear viscosity controls the magnitude of backscattering around the resonance frequency, where a target becomes a strong acoustic reflector. However, there is little information on the flesh shear viscosity values of fish, especially when it comes to mesopelagic species. Broadband acoustics provides the *TS* over a range of frequencies, compared to the few, widely spaced discrete frequencies in narrowband acoustics. Therefore, the estimated parameters from curve fitting to the broadband data are expected to be more accurate and reliable.

The viscous–elastic gas-filled spherical backscattering model (Feuillade and Nero, 1998; Khodabandeloo *et al.*, 2021a) was used for the inversion. The deviation from a spherical shape shifts the resonance to the higher frequencies (Figure 2) and the shift for a prolate spheroid with a given aspect ratio can be calculated (see Equation (S1)). For example, the resonance frequency of a prolate spheroid with the aspect ratios of 2 and 5 (ϵ = 0.5 and 0.2, respectively) compared to that of a sphere with the same volume is increased by around 2 and 11%, respectively. Other than the resonance frequency shift, the resonant backscattering shape and *TS*

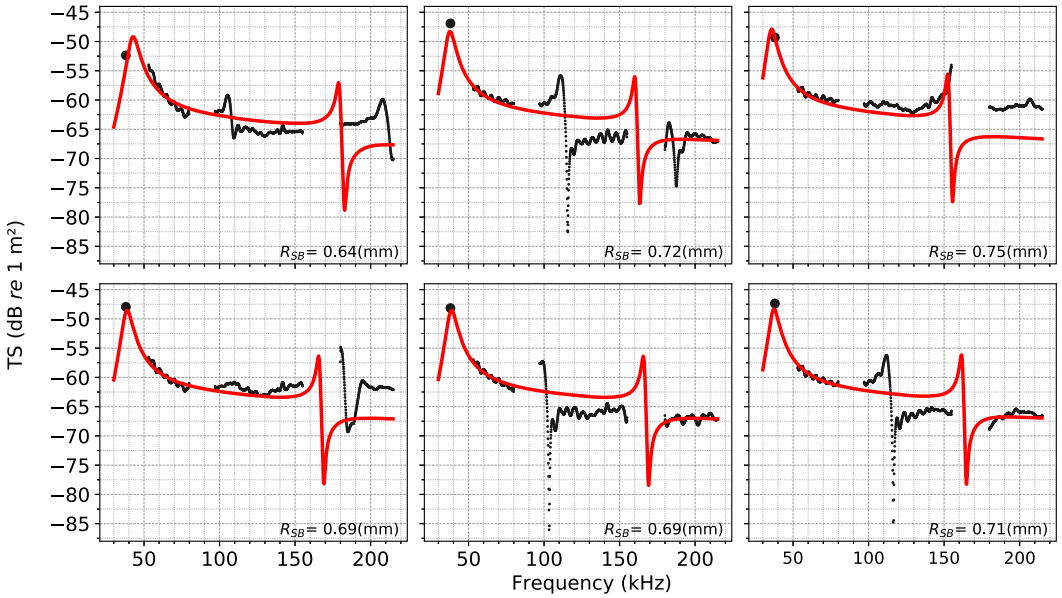

Figure 10. Selected larger targets ($N = 6$) with resonance below 53 kHz (the lower limit of 70-kHz broadband channel used in this paper). R_{SB} was the only tunable parameter and μ_f is determined per Equation (3). Measured and modeled *TS*s are shown by black dots and red line, respectively.

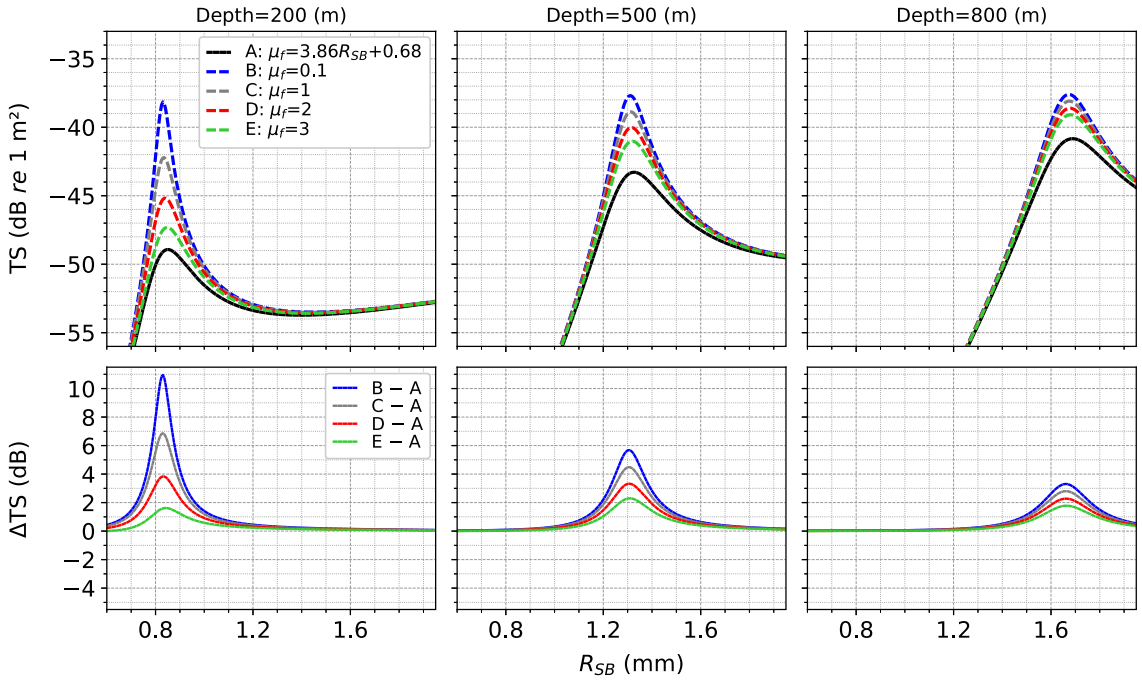

Figure 11. Top panels: estimated *TS* at 18 kHz for a range of swimbladder sizes for three different depths using different flesh shear viscosity values: (A) model given by Equation (3); (B–E): constant values. Bottom panels: difference (ΔTS) between *TS* for curves B to E and A.

amplitude are not strongly affected by the shape of swimbladder (Figure 2). The radius of a sphere with the same resonance as an elongated volume is less than the equivalent spherical radius of the elongated volume. In other words, the obtained radius from the inversion of spherical backscattering model is underestimated if the measured backscattering is from a non-spherical swimbladder. A prolate spheroid example would be helpful to quantify the underestimation of the radius derived from fitting the resonance of spherical model to a non-spherical swimbladder. The resonance frequency of a spherical bubble with radius R_0 can be estimated as

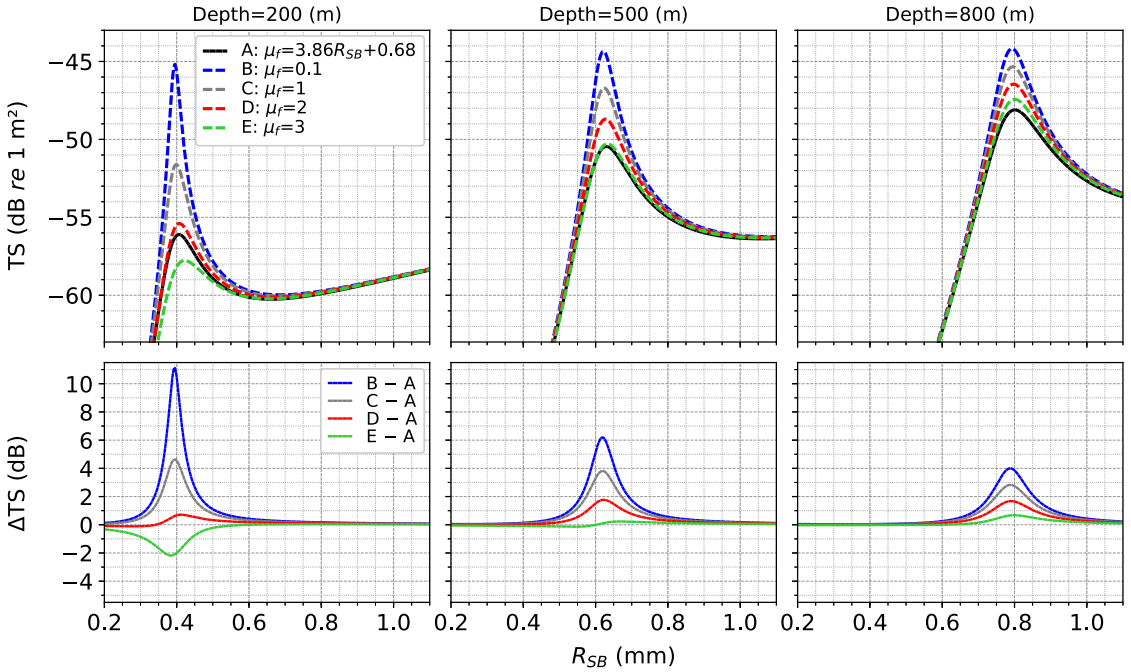

Figure 12. Top panels: estimated *TS* at 38 kHz for a range of swimbladder sizes for three different depths using different flesh shear viscosity values: (A) model given by Equation (3); (B–E): constant values. Bottom panels: difference (ΔTS) between *TS* for curves B to E and A.

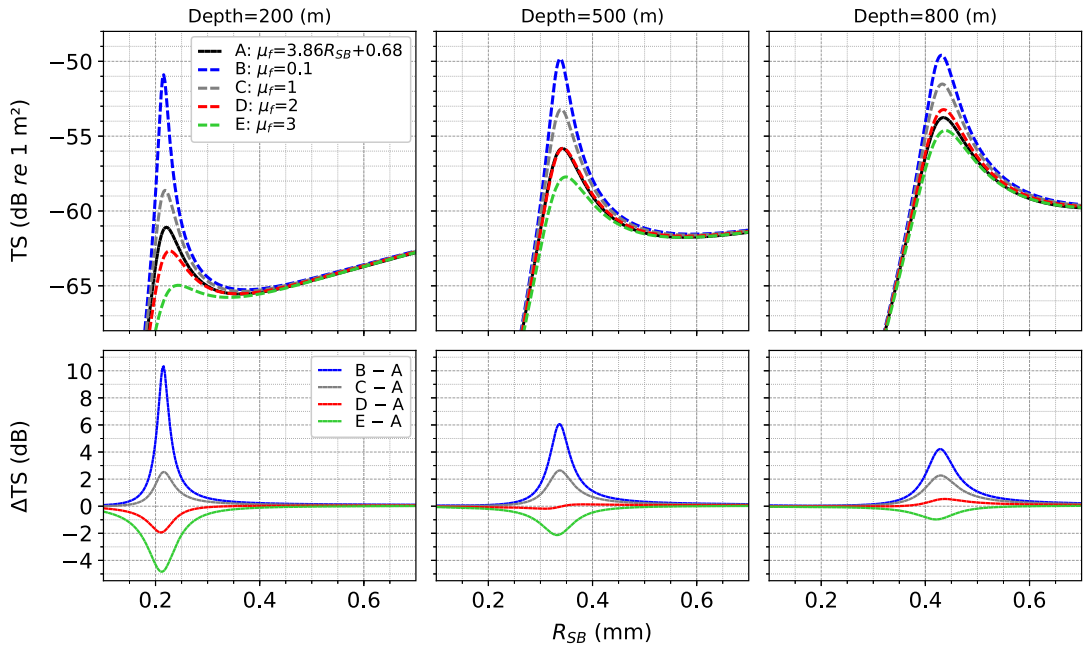

Figure 13. Top panels: estimated *TS* at 70 kHz for a range of swimbladders sizes for three different depths using different flesh shear viscosity values: (A) model given by Equation (3); (B–E): constant values. Bottom panels: difference (ΔTS) between *TS* for curves B to E and A.

(Minnaert, 1933; Strasberg, 1953)

$$\omega_0 = \frac{1}{R_0}\sqrt{\frac{3\gamma P_0}{\rho_w}}, \tag{6}$$

where γ is the specific heat ratio and P_0 is the pressure inside the bubble. Subsequently, the following relation can be obtained for a bubble at the same condition but with different size:

$$1 - \frac{\omega_2}{\omega_0} = \frac{R_2 - R_0}{R_2}, \tag{7}$$

where ω_2 is the resonance frequency of spherical bubble with radius R_2. On the other hand, Equation (S1) can be rewritten as

$$1-\frac{\omega_{0\epsilon}}{\omega_0}=1-2^{1/2}\epsilon^{-1/3}\left(1-\epsilon^2\right)^{-1/4}\left\{\ln\left[\frac{1+\left(1-\epsilon^2\right)^{\frac{1}{2}}}{1-\left(1-\epsilon^2\right)^{\frac{1}{2}}}\right]\right\}^{-1/2}, \tag{8}$$

where ϵ is the prolate spheroid's minor-to-major-axis. Subsequently, if the resonance of ellipsoid is fitted by the smaller sphere, i.e. $\omega_2=\omega_{0\epsilon}$, then from Equations (7) and (8), the following relation can be obtained:

$$\frac{R_2-R_0}{R_2}=1-2^{1/2}\,\epsilon^{-1/3}\left(1-\epsilon^2\right)^{-1/4}\left\{\ln\left[\frac{1+\left(1-\epsilon^2\right)^{1/2}}{1-\left(1-\epsilon^2\right)^{1/2}}\right]\right\}^{-1/2}. \tag{9}$$

Using Equation (9), the underestimation (in percentage) of the equivalent spherical radius is plotted (Figure 14) for different values of ϵ.

The underestimated swimbladder radius can cause underestimation of the flesh shear viscosity derived from the spherical model. This is observed by the dependence of the estimated flesh shear viscosities to the swimbladder wall thickness (i.e. Δ) in Figure 8 : The thicker the wall is, the higher the estimated flesh shear viscosity will be. If the shape (or elongation) of swimbladders was known, it might be better to use a Δ that depends on the R_{SB} (see Figure 14) to compensate the underestimation of R_0. Using this approach, flesh shear viscosity is estimated for different added thicknesses, $\Delta'(=R_0-R_2)$, as a percentage of R_{SB} (Figure 15) to the assumed swimbladder wall thickness (here 20×10^{-6} m). In other words, Δ is updated as

$$\Delta=\Delta'+20\times10^{-6}, \tag{10}$$

where Δ' compensates the underestimated spherical radius, R_2, for the elongated swimbladder (Figure 14). For example, for $\epsilon=\sim0.35$ (i.e. aspect ratio of ~2.9), the underestimation of the equivalent spherical radius and flesh shear viscosity is around 5% (Figure 14) and 15% (Figure 15), respectively.

Based on the above analysis, elongation factor can be included in the flesh shear viscosity model (Equation (3)) obtained from the spherical model as

$$\mu_{f\epsilon}=\left(1+1.65e^{-6.9\epsilon}\right)\times\mu_f, \tag{11}$$

where $\mu_{f\epsilon}$ is the flesh shear viscosity with the elongation factor correction and μ_f is given by Equation (3) or Equation (4). Different combinations of swimbladder wall shear elasticity and thickness were used to fit the model to the measurements and the quality of the fittings were compared (see the section "Model-fitting to *in situ TS* measurements for flesh shear viscosity estimation" and Figure 8). The results indicate that for the analysed targets the swimbladder wall thickness of 20 microns provides, overall, the better fit regardless of flesh elasticity value. Furthermore, it was observed that the swimbladder wall thickness and elasticity effects on the backscattering become less important for deep targets compared to the shallow ones (Figure 5).

The analysis indicates that flesh shear viscosity is swimbladder size dependent (see Equation (3) or Equation (4) with error term). Furthermore, it is observed that the linear regression model has a small R-squared value, which is caused by the broad range of flesh viscosities even among the same fish species (Løvik and Hovem, 1979). The flesh shear viscosity model was obtained using the targets with resonance within the measured broadband frequencies (Figure 7). The obtained flesh shear viscosity model was examined for larger targets that have resonance at lower frequencies, and it was observed that it provides reasonable fit for them as well (Figure 10). In addition, the obtained flesh shear viscosity values for a small ($R_{SB}=0.2$ mm) and a large ($R_{SB}=0.75$ mm) targets are around 1.45 ± 0.57 and 3.57 ± 0.57 kg m^{-1} s^{-1}, respectively, which lie within the range of reported values for vertebrates measured with different methods (see Table 2).

Finally, the effects of shear viscosity on the backscattering are investigated at 18, 38, and 70 kHz, the most common hull-mounted frequencies capable of reaching the mesopelagic layers from the surface. It is observed that the range of *TS* values estimated by varying the flesh shear viscosity is larger at shallower depths (Figures 11–13), i.e. the potential effects of an error in the shear viscosity are likely to be larger for shallow targets. In a study modelling the uncertainty ranges of acoustic mesopelagic biomass estimates, Proud *et al.* (2019) used a default value of 4/3 kg m^{-1} s^{-1} for shear viscosity, which would correspond to very small swimbladders in our study (Equation (3)). They did, however, perform a sensitivity analysis, testing a range of values, concluding that even if shear viscosity was important to *TS*, it was overall less important to their estimates of uncertainty in global biomass levels than other factors they tested. However, as a high value of this parameter effectively removes the effects of resonance on *TS* (Proud *et al.*, 2019), it is an essential parameter in modelling *TS* levels for mesopelagic fish species with gas-inclusions (Scoulding *et al.*, 2015). Consequently, as models of resonant scattering are being used with increasing frequency to estimate *TS* levels for mesopelagic fishes (Kloser *et al.*, 2002; Davison *et al.*, 2015a; Ariza *et al.*, 2016; Proud *et al.*, 2019; Sobradillo *et al.*, 2019), parameter input to these models should be tuned to be accurate for the organisms being studied. The results document that flesh shear viscosity has a large effect on the *TS* amplitude close to the resonant frequency. However, whether this results in large effects in the measured backscatter will depend on both the *in situ* size of the targets and their vertical distribution.

Conclusions

While flesh shear viscosity influences the backscattering amplitude around the resonance frequency of organisms with gas-inclusion, such as swimbladdered fish, there is limited information regarding mesopelagic species. Resonance frequency of swimbladdered mesopelagic fish can occur at higher frequencies, and resonance peaks in the collected *in situ* data were observed up to around 100 kHz, caused by small sizes of gas-inclusions and/or large depth of occurrence. Since the mesopelagic species can have resonance within the acoustic measurement frequencies, the knowledge of flesh shear viscosity becomes more pivotal for mesopelagic than for epipelagic fish to convert acoustic data into biomass. By applying a viscous–elastic model to *in situ* broadband backscattering measurements, we provide *in situ* estimates of flesh shear viscosity of swimbladdered mesopelagic fish. The results suggest that the flesh shear viscosity depends on the swimbladder size, and an empirical model (see Equation (3) or Equation (4)) is provided in this regard. Subsequently, the effects of swimbladder elongation were discussed and included in the estimated flesh shear viscosity (Equation (11)). Having a correct shear viscosity parameter provides a better *TS* model and hence reduces the uncertainties and biases when converting acoustic data into abundances and biomass.

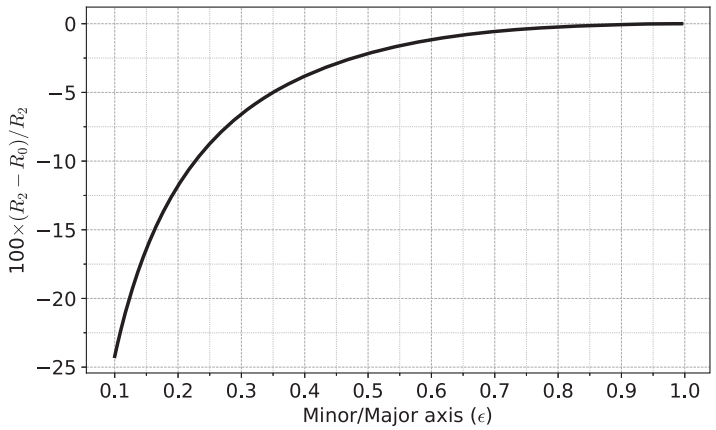

Figure 14. Underestimation (%, cf. Equation(9)) of equivalent spherical radius obtained from fitting resonance of spherical model to that of a prolate spheroid. *X*-axis shows the minor-to-major-axis ratios of prolate spheroid.

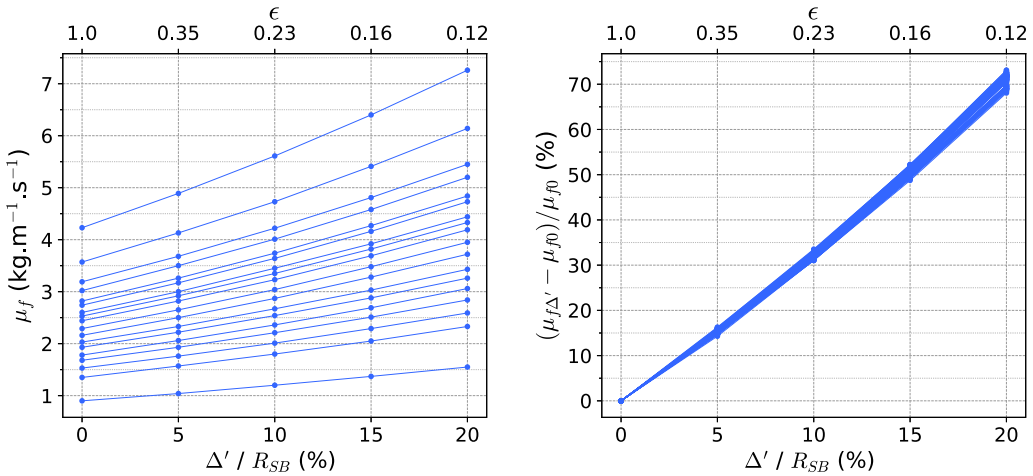

Figure 15. (Left) Estimated flesh shear viscosities for different values of added thickness (Δ') to R_{SB} represented by the percentage of Δ'/R_{SB}. Corresponding minor-to-major-axis ratio, ϵ, is obtained from Figure 14 and shown on the top axis. (Right) Percentage of change of estimated flesh shear viscosity, $\mu_{f\Delta'}$, from an elongated prolate spheroid compared to that of from an sphere, μ_{f0}, i.e., percentage of underestimation of flesh shear viscosity of an elongated swimbladder (see ϵ on top axis) using a spherical swimbladder model.

Table 2. Reported shear viscosity for different vertebrate tissues and their measurement method.

Species/organ	Shear viscosity (kg m^{-1} s^{-1})	Method
Maurolicus muelleri (Small and large)	1; Scoulding *et al.* (2015)	Acoustic multifrequency (narrowband)
Benthosema glaciale	3; Scoulding *et al.* (2015)	Acoustic multifrequency (narrowband)
Bovine muscle (along and across the fibres)	9.9 and 0.7; Chen *et al.* (2009)	Shearwave Dispersion Ultrasound Vibrometry (SDUV) method
Swine liver (*in vivo*)	1.95 $\pm$ 0.34; Chen *et al.* (2009)	SDUV method
Normal human liver (*in vivo*)	1.72 $\pm$ 0.15; Huwart *et al.* (2006)	Magnetic Resonance Elastography (MRE)
Normal rat liver	0.51 $\pm$ 0.04; Salameh *et al.* (2007)	MRE
Human liver	0.2–2.8; Yang (2018)	Time-domain measurements of shear waves in viscoelastic media

Supplementary data

Supplementary material is available at the *ICESJMS* online version of the manuscript.

Data availability statement

Data available on request. The data underlying this article will be shared on reasonable request to the corresponding author.

Acknowledgements

Funding for this work was provided by the Institute of Marine Research (project number 15093), HARMES project, Research Council of Norway (project number 280546), MEESO, EU H2020 research and innovation programme (grant agreement number 817669), and Center for Research-based Innovation in Marine Acoustic Abundance Estimation and Backscatter Classification (CRIMAC; number 309512).

References

Alvheim, A. R., Kjellevold, M., Strand, E., Sanden, M., and Wiech, M. 2020. Mesopelagic species and their potential contribution to food and feed security—a case study from Norway. Foods, 9: 344.

Anderson, V. C. 1950. Sound scattering from a fluid sphere. The Journal of the Acoustical Society of America, 22: 426–431.

Antona, A. 2016. Remote Fish Species and Size Identification Using Broadband Echosounders. Institute for Marine Resources and Ecosystem Studies (IMARES), Wageningen University.

Ariza, A., Landeira, J. M., Escánez, A., Wienerroither, R., Aguilar de Soto, N., Røstad, A., Kaartvedt, S. *et al.* 2016. Vertical distribution, composition and migratory patterns of acoustic scattering layers in the Canary Islands. Journal of Marine Systems, 157: 82–91.

Baidakov, V. G., Protsenko, S. P., and Kozlova, Z. R. 2011. Shear and bulk viscosity in stable and metastable states of a Lennard-Jones liquid. Chemical Physics Letters, 517: 166–170.

Baik, K. 2013. Comment on 'Resonant acoustic scattering by swimbladder-bearing fish' The Journal of the Acoustical Society of America, 133: 5–8; The Journal of the AcousticalSociety of America 64: 571–580 (1978) (L).

Bonomo, A. L., and Isakson, M. J. 2016. Modeling the acoustic scattering from axially symmetric fluid, elastic, and poroelastic objects due to nonsymmetric forcing using COMSOL Multiphysics. *In* Proceedings of the 2016 COMSOL Conference, Boston.

Cakoni, F., and Colton, D. 2005. Qualitative Methods in Inverse Scattering Theory: An Introduction, Springer Science & Business Media, 246pages.

Chen, S., Urban, M.W., Pislaru, C., Kinnick, R., Zheng, Y., Yao, A., and Greenleaf, J. 2009. Shearwave dispersion ultrasound vibrometry (SDUV) for measuring tissue elasticity and viscosity. IEEE Transactions on Ultrasonics, Ferroelectrics and Frequency Control, 56: 55–62.

Chu, D. 2011. Technology evolution and advances in fisheries acoustics. Journal of Marine Science and Technology, 19: 9.

Davison, P. C., Checkley, D. M., Koslow, J. A., and Barlow, J. 2013. Carbon export mediated by mesopelagic fishes in the northeast Pacific Ocean. Progress in Oceanography, 116: 14–30.

Davison, P. C., Koslow, J. A., and Kloser, R. J. 2015. Acoustic biomass estimation of mesopelagic fish: backscattering from individuals, populations, and communities. ICES Journal of Marine Science, 72: 1413–1424.

Davison, P., Lara-Lopez, A., and Anthony Koslow, J. 2015. Mesopelagic fish biomass in the southern California current ecosystem. Deep Sea Research Part II: Topical Studies in Oceanography, 112: 129–142.

Faran, J. J. J. 1951. Sound scattering by solid cylinders and spheres. The Journal of the Acoustical Society of America, 23: 405–418.

Feuillade, C., and Nero, R. W. 1998. A viscous-elastic swimbladder model for describing enhanced-frequency resonance scattering from fish. The Journal of the Acoustical Society of America, 103: 3245–3255.

Foote, K. G. 1980. Importance of the swimbladder in acoustic scattering by fish: a comparison of gadoid and mackerel target strengths. The Journal of the Acoustical Society of America, 67: 2084–2089.

García-Seoane, E., Wienerroither, R., Mork, K. A., Underwood, M. J., and Melle, W. 2021. Biogeographical patterns of meso- and bathypelagic fish along a Northeastern Atlantic transect. ICES Journal of Marine Science, 78: 1444–1457.

Gjoesaeter, J., and Kawaguchi, K. 1980. A Review of the World Resources of Mesopelagic Fsh. FAO Fisheries Technical Papers (FAO). https://agris.fao.org/agris-search/search.do?recordID=XF8003729 (last accessed date March 2021).

Hickling, R. 1962. Analysis of echoes from a solid elastic sphere in water. The Journal of the Acoustical Society of America, 34: 1582–1592.

Horne, J. K. 2000. Acoustic approaches to remote species identification: a review. Fisheries Oceanography, 9: 356–371.

Huwart, L., Peeters, F., Sinkus, R., Annet, L., Salameh, N., ter Beek, L.C., Horsmans, Y. *et al.* 2006. Liver fibrosis: non-invasive assessment with MR elastography. NMR in Biomedicine, 19: 173–179.

Ida, N. 1983. Three Dimensional Finite Element Modeling of Electromagnetic Nondestructive Testing Phenomena (Doctoral dissertation), Colorado State University.

Irigoien, X., Klevjer, T. A., Røstad, A., Martinez, U., Boyra, G., Acuña, J. L., Bode, A. *et al.* 2014. Large mesopelagic fishes biomass and trophic efficiency in the open ocean. Nature Communications, 5: 3271.

Jech, J. M., Horne, J. K., Chu, D., Demer, D. A., Francis, D. T. I., Gorska, N., Jones, B. *et al.* 2015. Comparisons among ten models of acoustic backscattering used in aquatic ecosystem research. The Journal of the Acoustical Society of America, 138: 3742–3764.

Jones, E., Oliphant, T., and Peterson, P. 2001. *SciPy: Open source scientific tools for Python.* http://www.scipy.org/ (last accessed 8 February 2021).

Kaartvedt, S., Staby, A., and Aksnes, D. L. 2012. Efficient trawl avoidance by mesopelagic fishes causes large underestimation of their biomass. Marine Ecology Progress Series, 456: 1–6.

Khodabandeloo, B., Agersted, M. D., Klevjer, T., Macaulay, G. J., and Melle, W. 2021a. Estimating target strength and physical characteristics of gas-bearing mesopelagic fish from wideband in situ echoes using a viscous-elastic scattering model. The Journal of the Acoustical Society of America, 149: 673–691.

Khodabandeloo, B., Ona, E., Macaulay, G. J., and Korneliussen, R. 2021b. Nonlinear crosstalk in broadband multi-channel echosounders. The Journal of the Acoustical Society of America, 149: 87–101.

Klevjer, T. A., Torres, D. J., and Kaartvedt, S. 2012. Distribution and diel vertical movements of mesopelagic scattering layers in the Red Sea. Marine Biology, 159: 1833–1841.

Kloser, R. J., Ryan, T. E., Young, J. W., and Lewis, M. E. 2009. Acoustic observations of micronekton fish on the scale of an ocean basin: potential and challenges. ICES Journal of Marine Science, 66: 998–1006.

Kloser, R. J., Ryan, T., Sakov, P., Williams, A., and Koslow, J. A. 2002. Species identification in deep water using multiple acoustic frequencies. Canadian Journal of Fisheries and Aquatic Sciences, 59: 13.

Knutsen, T., Melle, W., Mjanger, M., Strand, E., Fuglestad, A.-L., Broms, C., Bagøien, E. *et al.* 2013. MESSOR – a towed underwater vehicle for quantifying and describing the distribution of pelagic organisms and their physical environment. *In* Proceedings of the 2013 MTS/IEEE OCEANS conference, pp. 1–12. doi:10.1109/OCEANS-Bergen.2013.6608177.

Lavery, A. C., Wiebe, P. H., Stanton, T. K., Lawson, G. L., Benfield, M. C., and Copley, N. 2007. Determining dominant scatterers of sound in mixed zooplankton populations. The Journal of the Acoustical Society of America, 122: 3304–3326.

Love, R. H. 1978. Resonant acoustic scattering by swimbladder-bearing fish. The Journal of the Acoustical Society of America, 64: 571–580.

Løvik, A., and Hovem, J. M. 1979. An experimental investigation of swimbladder resonance in fishes. The Journal of the Acoustical Society of America, 66: 850–854.

Marshall, N. B. 1960. Swimbladder Structure of Deep-Sea Fishes in Relation to their Systematics and Biology (Discovery Reports), 27, pp. 1–121.Cambridge University Press.

Medwin, H. 2005. Sounds in the Sea: From Ocean Acoustics to Acoustical Oceanography. Cambridge University Press, Cambridge.

Minnaert, M. 1933. On musical air-bubbles and the sounds of running water. The London, Edinburgh, and Dublin Philosophical Magazine and Journal of Science, 16: 235–248.

Nelson, J. S., Grande, T. C., and Wilson, M. V. H. 2016. Fishes of the World. John Wiley & Sons, Inc., Hoboken, NJ.

Ona, E. 1999. Methodology for Target Strength Measurements (With Special Reference to In Situ Techniques for Fish and Micro-Nekton). ICES Cooperative Research Report 235, p. 59.

Priede, I. G. 2017. Deep-Sea Fishes: Biology, Diversity, Ecology and Fisheries., Cambridge University Press.

Proud, R., Handegard, N. O., Kloser, R. J., Cox, M. J., and Brierley, A. S. 2019. From siphonophores to deep scattering layers: uncertainty ranges for the estimation of global mesopelagic fish biomass. ICES Journal of Marine Science, 76: 718–733.

R. Massel, S. 2015. Internal Gravity Waves in the Shallow Seas (Geo-Planet: Earth and Planetary Sciences), Springer International Publishing, Cham.

Reeder, D. B., Jech, J. M., and Stanton, T. K. 2004. Broadband acoustic backscatter and high-resolution morphology of fish: measurement and modeling. The Journal of the Acoustical Society of America, 116: 747–761.

Robinson, C., Steinberg, D. K., Anderson, T. R., Arístegui, J., Carlson, C. A., Frost, J. R., Ghiglione, J.-F. *et al.* 2010. Mesopelagic zone ecology and biogeochemistry—a synthesis. Deep Sea Research Part II: Topical Studies in Oceanography, 57: 1504–1518.

Ross, L. G. 1976. The permeability to oxygen of the swimbladder of the mesopelagic fish Ceratoscopelus maderensis. Marine Biology, 37: 83–87.

Salameh, N., Peeters, F., Sinkus, R., Abarca-Quinones, J., Annet, L., ter Beek, L. C., Leclercq, I. *et al.* 2007. Hepatic viscoelastic parameters measured with MR elastography: correlations with quantitative analysis of liver fibrosis in the rat. Journal of Magnetic Resonance Imaging, 26: 956–962.

Scoulding, B., Chu, D., Ona, E., and Fernandes, P. G. 2015. Target strengths of two abundant mesopelagic fish species. The Journal of the Acoustical Society of America, 137: 989–1000.

Simmonds, J., and MacLennan, D. 2005. Fisheries Acoustics. Theory and Practice, 2nd edn., pp. 437 Blackwell Science, Oxford.

Sobradillo, B., Boyra, G., Martinez, U., Carrera, P., Peña, M., and Irigoien, X. 2019. Target strength and swimbladder morphology of Mueller's pearlside (*Maurolicus muelleri*). Scientific Reports, 9: 17311.

Stanton, T. K., Chu, D., Jech, J. M., and Irish, J. D. 2010. New broadband methods for resonance classification and high-resolution imagery of fish with swimbladders using a modified commercial broadband echosounder. ICES Journal of Marine Science, 67: 365–378.

Stanton, T. K., Wiebe, P. H., and Chu, D. 1998. Differences between sound scattering by weakly scattering spheres and finite–length cylinders with application to sound scattering by zooplankton. The Journal of the Acoustical Society of America, 103: 254–264.

Strasberg, M. 1953. The pulsation frequency of nonspherical gas bubbles in liquids. The Journal of the Acoustical Society of America, 25: 536–537.

Weisberg, S. 2014. Applied Linear Regression, 4th edn. John Wiley & Sons.

Yang, Y. 2018. Shear Elasticity And Shear Viscosity Imaging In Soft Tissue. Michigan State University.

Ye, Z. 1997. Low-frequency acoustic scattering by gas-filled prolate spheroids in liquids. The Journal of the Acoustical Society of America, 101: 1945–1952.

Zampolli, M., Tesei, A., Jensen, F., Malm, N., and Blottman, J. III 2007. A computationally efficient finite element model with perfectly matched layers applied to scattering from axially symmetric objects. The Journal of the Acoustical Society of America, 122: 1472–1485.

Handling Editor: David Demer